

Modeling Pairwise Peculiar Velocity Distribution Function of Dark Matter from Halo Density Profiles

Takeshi KUWABARA,¹ Atsushi TARUYA,^{1,2} and Yasushi SUTO^{1,2}

¹*Department of Physics, School of Science, University of Tokyo, Tokyo 113-0033*

²*Research Center for the Early Universe (RESCEU),*

School of Science, University of Tokyo, Tokyo 113-0033

kuwabara@utap.phys.s.u-tokyo.ac.jp, ataruya@phys.s.u-tokyo.ac.jp,

suto@phys.s.u-tokyo.ac.jp

(Received 2001 November 28; accepted 2002 May 2)

Abstract

We derive the pairwise peculiar velocity distribution function of dark matter particles applying the dark matter halo approach. Unlike the previous work, we do not assume a Gaussian velocity distribution function of dark matter in a single halo, but compute it self-consistently with the assumed density profile for dark matter halo. The resulting distribution function is well approximated by an exponential distribution which is consistent with the previous observational, numerical and theoretical results. We also compute the pairwise peculiar velocity dispersion for different density profiles, and provide a practical fitting formula. We apply an empirical biasing scheme into our model and present prediction for pairwise peculiar velocity dispersion of *galaxies*, and reproduce the previous results of simulations using our semi-analytical method.

Key words: cosmology:theory—dark matter—large-scale structure of universe

1. Introduction

Since Davis & Peebles (1983) first analyzed the anisotropy in the galaxy distribution from Center for Astrophysics (CfA) redshift catalog, it has been recognized that the peculiar velocity field of galaxies induces a significant systematic effect in statistics of observed galaxy distributions in redshift space. In particular, virialized random motion of galaxies produces an elongated pattern of galaxy distribution along the line of sight, called *finger-of-God*. This effect significantly suppresses the amplitude of the two-point correlation function of galaxies in redshift space, especially on scales below $\sim 3h^{-1}\text{Mpc}$.

The proper account of this redshift-space distortion requires a detailed model for the pairwise velocity distribution function (hereafter, PVDF) of galaxies. Davis & Peebles (1983)

discovered that the PVDF of the CfA galaxy sample is approximately described by an exponential distribution, instead of a Gaussian:

$$f_{12}(v_{12}; r_{12}) = \frac{1}{\sqrt{2}\sigma_{12}(r_{12})} \exp\left(-\frac{\sqrt{2}v_{12}}{\sigma_{12}(r_{12})}\right), \quad (1)$$

where r_{12} is the separation length and v_{12} denote the pairwise peculiar velocity between a pair of galaxy along the line-of-sight direction. The quantity $\sigma_{12}(r_{12})$ is the peculiar velocity dispersion (PVD). The exponential form of PVDF was confirmed also later by analyses of N -body simulations of dark matter particles and of other samples of galaxies (e.g., Efstathiou et al. 1988, Fisher et al. 1994, Marzke et al. 1995).

Theoretical models for the origin of the exponential PVDF of dark matter were put forward by Sheth (1996) and Diaferio & Geller (1996), and more recently by Sheth & Diaferio (2001). They phenomenologically introduced a nonlinear model of PVDF using the Press–Schechter formalism. To be more specific, they assume that any dark matter particle belongs to one of virialized clumps (dark halos) with the 1-point velocity distribution function being a Maxwellian form. If one considers sufficiently small scales, the particle pairs of those separations are likely to be in the same halo, and then their PVDF is approximately given by

$$f_{12}(v_{12}; r_{12}) = \frac{\int dM n(M) N_{\text{pair}}(r_{12}|M) f_{12,1h}(v_{12}|M)}{\int dM n(M) N_{\text{pair}}(r_{12}|M)}, \quad (2)$$

where $n(M)$ is the mass function of dark halos, $f_{12,1h}(v_{12}|M)$ is the PVDF of dark matter particles within a halo of mass M . The quantity $N_{\text{pair}}(r_{12}|M)$ represents the statistical weight proportional to the number of particle pairs with separation r_{12} in the halo:

$$N_{\text{pair}}(r_{12}|M) = \int d\mathbf{r}_1^3 \int d\mathbf{r}_2^3 \rho(\mathbf{r}_1|M) \rho(\mathbf{r}_2|M) \delta_D(r_{12} - |\mathbf{r}_1 - \mathbf{r}_2|), \quad (3)$$

where $\rho(r|M)$ is the density profile of the halo of mass M , and δ_D is the Dirac delta function. Adopting the singular isothermal distribution as a particular choice of the dark halo profile, Sheth (1996) showed that the scale-free model of $P(k) \propto k^n$ with $n = -1$ exactly reproduces the exponential PVDF (1).

While a perturbation theory (Seto & Yokoyama 1998; Juszkiewicz et al. 1998) also qualitatively explained why the Gaussian initial models approach the exponential PVDF, the above model is much more successful quantitatively. Further, a significant influence of the finger-of-Got effect appears at small scale, where the perturbative approach cannot be applied. Therefore in the present paper, we attempt to improve the Sheth (1996) model (2) for the PVDF in several aspects; first, we consider more popular CDM models instead of the scale-free power-spectra. Second, we adopt a series of more realistic density profiles for dark halos (Hernquist 1990; Navarro, Frenk & White 1997; Fukushige & Makino 1997, 2001a; Moore et al. 1998; Jing & Suto 2000). Third, we derive the one-point PVDF of dark matter particles in a halo directly from the Abel integral of the above density profiles, instead of assuming the Maxwellian form

a priori. This approach is important since we can incorporate the scale- and mass-dependence of the PVD in a consistent fashion unlike the previous modeling. Finally we also apply the selection function following Jing, Börner & Suto (2002) so as to phenomenologically attempt to predict the PVD of *galaxies* out of that of dark matter particles.

This paper is organized as follows; Section 2 describes our improved modeling for the PVDF on the basis of the dark matter halo approach. In §3, we present the resultant PVD in various cosmological models and discuss how the underlying halo profiles are sensitive to those results. We also provide a simple fitting formula of the PVD in the currently popular spatially-flat CDM model, which is useful in modeling the redshift-distortion effect. Then we attempt to consider the effect of the spatial biasing of galaxies relative to the dark matter particles on the PVD by applying a phenomenological biasing scheme. Finally section 4 is devoted to summary and conclusions.

2. A Dark Matter Halo Approach to Compute the Pairwise Velocity Distribution Function

Our present method to compute the PVDF is schematically shown in Figure 1. We will describe the details of the procedure below. Throughout the paper, we consider the three representative CDM models parameterized by the density parameter Ω_0 , the dimensionless cosmological parameter λ_0 , the amplitude of the mass fluctuation smoothed over the top-hat radius of $8h^{-1}\text{Mpc}$, σ_8 , and the Hubble constant in units of 100 km/s/Mpc h ; standard CDM ($\Omega_0 = 1.0, \lambda_0 = 0, \sigma_8 = 0.6, h = 0.5$; SCDM), lambda CDM ($\Omega_0 = 0.3, \lambda_0 = 0.7, \sigma_8 = 1.0, h = 0.7$; LCDM), and open CDM ($\Omega_0 = 0.45, \lambda_0 = 0, \sigma_8 = 0.83, h = 0.7$; OCDM). Those models are normalized to satisfy the X-ray cluster abundances (Kitayama & Suto 1997).

2.1. Density profile

The density profile of dark matter halos plays a key role in our method. Following the recent suggestions from high-resolution numerical simulations, we adopt the following specific form:

$$\rho(r|M) = \begin{cases} \frac{\bar{\rho}(z)\delta_c}{(r/r_s)^\alpha(1+r/r_s)^\nu} & (r < r_{\text{vir}}) \\ 0 & (r > r_{\text{vir}}) \end{cases} . \quad (4)$$

In the above, M is the mass of the halo, $\bar{\rho}(z) \equiv \Omega_0 \rho_{c0} (1+z)^3$ is the mean density of the universe at z , ρ_{c0} is the present critical density, $\delta_c(M)$ is the characteristic density excess, and $r_{\text{vir}}(M)$ and $r_s(M)$ indicate the virial radius and the scale radius of the halo, respectively.

The virial radius is defined according to the spherical collapse model as

$$r_{\text{vir}}(M) \equiv \left(\frac{3M}{4\pi\bar{\rho}\Delta_{\text{nl}}} \right)^{1/3} . \quad (5)$$

We use the following expressions (Kitayama & Suto 1996) for the critical over-density Δ_{nl} :

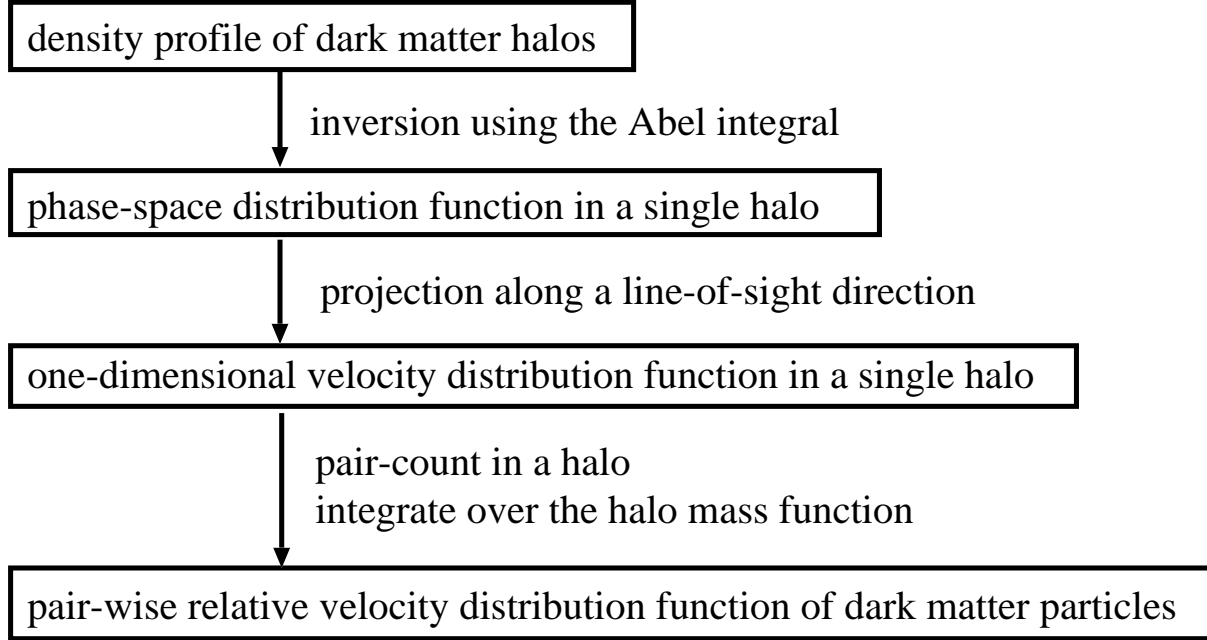


Fig. 1. Schematic illustration of our procedure to compute the pairwise velocity distribution function.

$$\Delta_{\text{nl}}(\Omega_0, \lambda_0) = \begin{cases} 18\pi^2(1 + 0.4093\omega_{\text{vir}}^{0.9052}) & (\Omega_0 < 1, \Omega_0 + \lambda_0 = 1) \\ 4\pi^2 \frac{(\cosh \eta_{\text{vir}} - 1)^2}{(\sinh \eta_{\text{vir}} - \eta_{\text{vir}})^2} & (\Omega_0 < 1, \lambda_0 = 0) \end{cases}, \quad (6)$$

where ω_{vir} and η_{vir} are respectively given as $\omega_{\text{vir}} \equiv 1/\Omega_{\text{vir}} - 1$ and $\eta_{\text{vir}} \equiv \cosh^{-1}(2/\Omega_{\text{vir}} - 1)$, in terms of the density parameter at the collapse time, Ω_{vir} .

In practice, we focus on three specific profiles. (i) the original NFW profile with $\alpha = 1$ and $\nu = 2$ (Navarro et al. 1997), (ii) the modified NFW profile with $\alpha = \nu = 3/2$ indicated by higher-resolution simulations (Fukushige & Makino 1997, 2001a,b; Moore et al. 1998; Jing & Suto 2000), (iii) the Hernquist profile with $\alpha = 1$ and $\nu = 3$ (Hernquist 1990) for which the analytic expression of the phase-space distribution function is known.

The two parameters r_s and r_{vir} are not independent, and are related in terms of the concentration parameter:

$$c(M, z) \equiv \frac{r_{\text{vir}}(M, z)}{r_s(M, z)}. \quad (7)$$

The condition that the total mass inside r_{vir} is equal to M relates δ_c to c . Therefore the halo mass-dependence of the above profiles is entirely specified by $c = c(M)$. In the case of the original NFW profile, we use the approximate fitting function from the simulation data of Bullock et al. (2001):

$$c_{\text{B}}(M) = \frac{8.0}{1+z} \left(\frac{M}{10^{14} M_{\odot}} \right)^{-0.13}. \quad (8)$$

For the other profiles, we first compute the amplitude of the two-point correlation functions

of dark matter following the procedure of Seljak (2000) and Ma & Fry (2000), and then find the amplitude of the concentration parameter which reproduces the Peacock – Dodds (1996) fitting formula. This calibration yield $c(M) = c_B(M)/2$ for the modified NFW profile (Oguri et al. 2001), and $c(M) = c_B(M)/3$ for the Hernquist profile, which we adopt throughout the analysis below.

2.2. Phase-space distribution function in a halo

Our next task is to compute the phase-space distribution function in a single halo from the given density profile (4). While Sheth (1996) and Sheth et al. (2001) simply adopt the Gaussian velocity distribution function, we eliminate this assumption and derive the velocity distribution function in a fully consistent manner.

For this purpose, we make use of the Jeans theorem which states that for a spherically symmetric and stationary system, the solution of the collisionless Boltzmann equation can be expressed as a function of the specific binding energy, $E = \psi(r) - v^2/2$, alone. Here we define ψ as the minus of the gravitational potential satisfying the boundary condition of $\psi(r \rightarrow \infty) \rightarrow 0$.

One may wonder whether halos in hierarchical universes that should experience repeated merger and destruction continually are well approximated as stationary. Nevertheless Natarajan, Hjorth & van Kampen (1997) and Hanyu & Habe (2001) found that the phase-space distribution function directly estimated from their particle simulations agrees well with that derived from the Jeans theorem. Thus the above assumption is justified, at least empirically.

Then the phase-space distribution function $F(E|M)$ in a single halo is directly computed from its given density profile $\rho(r|M)$ as follows (e.g., Binney & Tremaine 1987):

$$F(E|M) = \frac{1}{\sqrt{8}\pi^2} \frac{d}{dE} \int_0^E \frac{d\rho}{d\psi} \frac{d\psi}{\sqrt{E-\psi}}. \quad (9)$$

Figure 2 plots the dimensionless phase-space distribution function $f(\varepsilon) \equiv F(E|M)(Gm_s/r_s)^{3/2}/(\delta_c\bar{\rho})$ evaluated numerically from equation (9), where $m_s \equiv 4\pi r_s^3\delta_c\bar{\rho}$ is the characteristic mass of the halo and $\varepsilon = Er_s/(Gm_s)$ is the dimensionless specific energy. The Hernquist model has an analytical solution for $F(E|M)$ which is reproduced by our numerical result almost within an accuracy of 2% except for the tiny region $\varepsilon \sim 0$, where the error reaches at 7% but the effect is safely negligible for later analysis. Since the three halo profiles that we adopt have a central cusp, $f(\varepsilon)$ diverges at a corresponding value of ε . The modified NFW profile has $f(\varepsilon)$ which extends more broadly up to $\varepsilon \sim 2$ reflecting the stronger central concentration than that of the original NFW case.

2.3. Single-particle velocity distribution function in a halo

Once the phase-space distribution function is given, one can also compute one-dimensional single-particle velocity distribution function along a particular direction by integrating over the other two components. Assuming the isotropic velocity distribution, one has

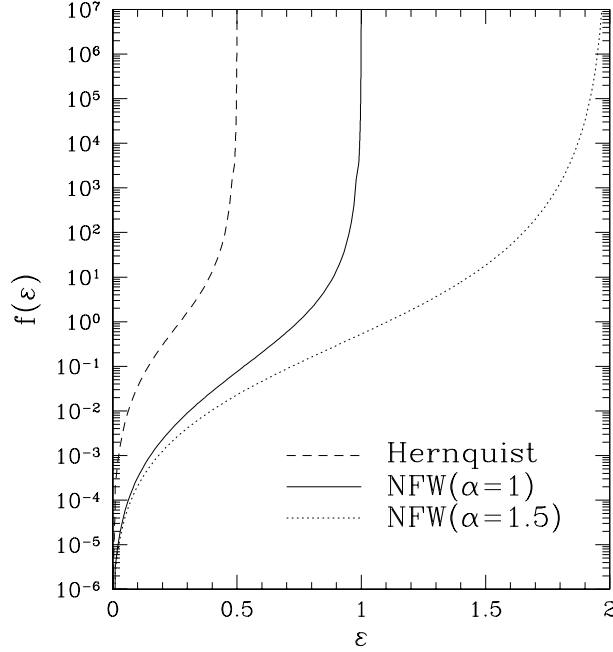


Fig. 2. The dimensionless phase-space distribution function $f(\varepsilon) \equiv F(E|M)(Gm_s/r_s)^{3/2}/(\delta_c \bar{\rho})$ as a function of dimensionless binding energy $\varepsilon = Er_s/(Gm_s)$; NFW($\alpha = 1$) profile (*solid*), NFW($\alpha = 1.5$) profile (*dotted*) and the Hernquist profile (*dashed*).

$$\begin{aligned}
 f_1(v_1|M;r) &\equiv \frac{1}{\rho(r|M)} \int dv_2 \int dv_3 F(E|M) \\
 &= \frac{1}{\sqrt{2\pi} \rho(r|M)} \int_0^{E_1} dE \frac{d}{dE} \int_0^E \frac{d\rho}{d\psi} \frac{d\psi}{\sqrt{E-\psi}} \\
 &= \frac{1}{\sqrt{2\pi} \rho(r|M)} \int_0^{E_1} \frac{d\rho}{d\psi} \frac{d\psi}{\sqrt{E-\psi}}, \tag{10}
 \end{aligned}$$

where we project along the direction of v_1 and the quantity $E_1 \equiv \psi - v_1^2/2$ is the corresponding binding energy. Figure 3 shows the dimensionless velocity distribution function $v_s f_1(v|M;r)$ at $r/r_s = 1$ (*thin lines*) and $r/r_s = 10$ (*thick lines*), where $v_s \equiv (Gm_s/r_s)^{1/2}$ is the scaling velocity. The figure indicates that the one-dimensional velocity distribution function in a halo can be reasonably approximated by the Gaussian:

$$f_1(v|M;r) = \frac{1}{\sqrt{2\pi}\sigma(r|M)} \exp\left(-\frac{v^2}{2\sigma^2(r|M)}\right), \tag{11}$$

although it has a sharp cutoff around the escape velocity of the halo, $v_{\text{esc}} = (2\psi)^{1/2}$.

In Figure 3, the dashed lines indicate the Gaussian-fit which has the same velocity dispersion evaluated from equation (10). It seems that the empirical Gaussian approximation can reasonably reproduce the PVDF, and thus we use the approximation in the numerical integrations below so as to reduce the computational time.

Figure 4 plots the velocity dispersion $\sigma(r|M)$ computed from the best-fit Gaussian, which clearly shows the scale-dependence that was neglected in the previous analysis (Sheth

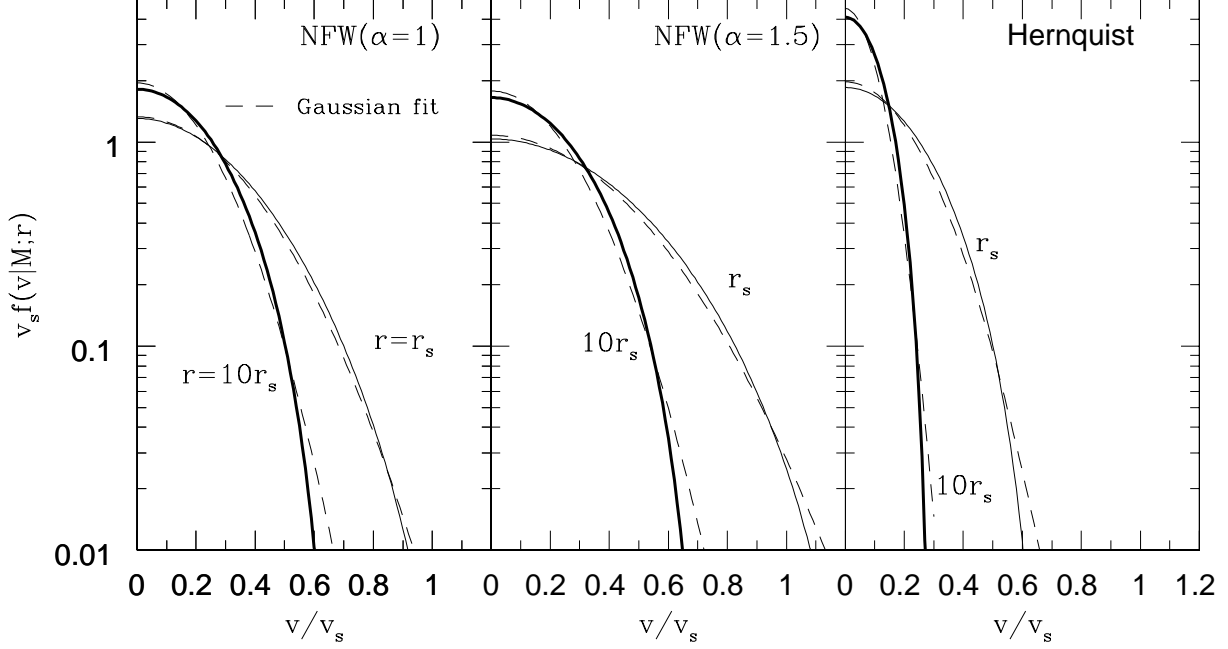


Fig. 3. Single-particle velocity distribution function in a single halo at $r/r_s = 1$ (*thin-solid*) and $r/r_s = 10$ (*thick-solid*). The dashed lines show the corresponding Gaussian fits (see eq.[11]). *Left:* NFW($\alpha = 1$); *Middle:* NFW($\alpha = 1.5$); *Right:* Hernquist profile.

1996; Sheth et al. 2001). Note also the different scale-dependence from the circular velocity $V_c \equiv Gm(r)/r$, where $m(r)$ is the mass inside the radius r (thin lines in Fig.4). In the subsequent modeling of the PVDF, we use the Gaussian approximation with the fitted $\sigma(r|M)$ rather than repeating the full numerical integration.

2.4. Pairwise relative velocity distribution function

Finally we are in a position to estimate the PVDF combining the above results. Since we are interested in small scales, the particle pairs with the corresponding separations are approximated to reside in the common halo. Then Sheth (1996) derived the following expression for the PVDF:

$$f(v_{12}; r_{12}) = \mathcal{N}^{-1} \int dM n(M) \int d^3\mathbf{r}_1 d^3\mathbf{r}_2 \rho(r_1|M) \rho(r_2|M) \times \int dv_1 dv_2 f_1(v_1|M; r_1) f_1(v_2|M; r_2) \delta_D(r_{12} - |\mathbf{r}_1 - \mathbf{r}_2|) \delta_D(v_{12} - v_1 + v_2), \quad (12)$$

where r_{12} is the pair-separation and \mathcal{N} is the normalization factor given by

$$\mathcal{N} = \int dM n(M) \int d^3\mathbf{r}_1 d^3\mathbf{r}_2 \rho(r_1|M) \rho(r_2|M) \delta_D(r_{12} - |\mathbf{r}_1 - \mathbf{r}_2|). \quad (13)$$

The relation between the quantities used in the expressions (12) and (13) are schematically summarized in Figure 5.

While Sheth (1996) adopted the singular isothermal sphere $\rho(r) \propto r^{-2}$ and therefore the Maxwellian for $f_1(v|M; r)$ with r -independent velocity dispersion, we are able to evaluate

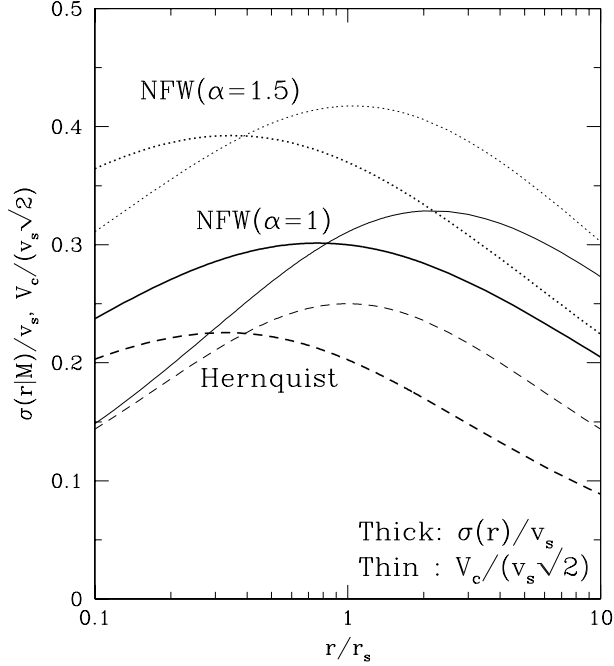


Fig. 4. The peculiar velocity dispersion $\sigma(r|M)$ of dark matter particles in a single halo resulting from the Gaussian fit as a function of position r/r_s (*thick lines*). For comparison, the thin lines show the circular velocity V_c evaluated from the relation $V_c(r) = Gm(r)/r$, where $m(r)$ represents the mass inside the radius r . Solid line, dotted line, and dashed lines represent the results in NFW($\alpha = 1$), NFW($\alpha = 1.5$), and Hernquist profiles, respectively.

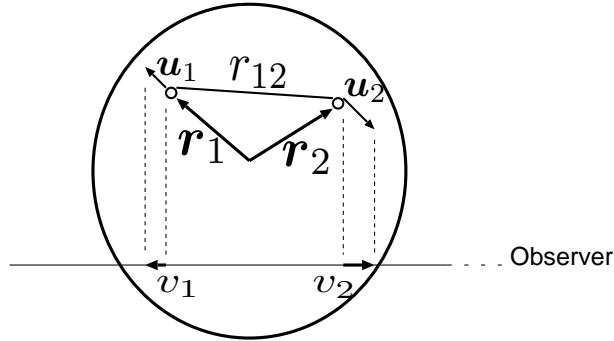


Fig. 5. The schematic picture of the relations of the relative positions and velocities used in the expressions (12) and (13). The large circle and the two small circles denote a halo and a pair of particles, respectively. The separation length of the pair r_{12} is defined by $|\mathbf{r}_1 - \mathbf{r}_2|$ and the relative pairwise velocity v_{12} is defined by $v_1 - v_2$. The quantities v_1 and v_2 are the line-of-sight component of the three dimensional velocities \mathbf{u}_1 and \mathbf{u}_2 , respectively.

equation (12) in more realistic situations as described in the preceding subsections.

Applying the Gaussian fit (eq.[11]) for $f_1(v|M;r)$, equation (12) is rewritten as

$$f_{12}(v_{12}|r_{12}) = \mathcal{N}^{-1} \int dM n(M) \int d^3\mathbf{r}_1 \int d^3\mathbf{r}_2 \frac{\rho(r_1|M) \rho(r_2|M)}{2\pi\sigma(r_1|M)\sigma(r_2|M)} \\ \times \int dv_1 dv_2 \exp \left[-\frac{v_1^2}{2\sigma^2(r_1|M)} - \frac{v_2^2}{2\sigma^2(r_2|M)} \right] \delta_D(r_{12} - |\mathbf{r}_1 - \mathbf{r}_2|) \delta_D(v_{12} - v_1 + v_2) \quad (14)$$

The integrals over the two velocity components v_1 and v_2 , and also over the directions of the position vectors can be performed analytically, and equation (14) reduces to

$$f_{12}(v_{12}|r_{12}) = \frac{\tilde{\mathcal{N}}^{-1}}{4\pi r_{12}^2 \bar{\rho}^2} \int_{M_{\min}(r_{12})}^{\infty} dM n(M) r_{12} \int_{\max(0, r_{12}-r_{sc})}^{r_{sc}} dr_2 \int_{|r_{12}-r_2|}^{\min(r_{sc}, r_{12}+r_2)} dr_1 \\ \times r_1 r_2 \frac{\rho(r_1|M) \rho(r_2|M)}{\sqrt{2\pi\{\sigma^2(r_1|M) + \sigma^2(r_2|M)\}}} \exp \left[-\frac{v_{12}^2}{2\{\sigma^2(r_1|M) + \sigma^2(r_2|M)\}} \right], \quad (15)$$

where $M_{\min}(r_{12})$ is the minimum mass of the halo including the pair with separation r_{12} (i.e., $r_{\text{vir}}(M_{\min}) > r_{12}/2$), and the normalization factor $\tilde{\mathcal{N}}$ is now given by

$$\tilde{\mathcal{N}} = \frac{1}{4\pi r_{12}^2 \bar{\rho}^2} \int_{M_{\min}(r_{12})}^{\infty} dM n(M) r_{12} \int_{\max(0, r_{12}-r_{sc})}^{r_{sc}} dr_2 \int_{|r_{12}-r_2|}^{\min(r_{sc}, r_{12}+r_2)} dr_1 r_1 r_2 \rho(r_1|M) \rho(r_2|M). \quad (16)$$

Actually it turns out that this term corresponds to the one-halo contribution of the two-point correlation function, $\xi_{1h}(r_{12})$, in the dark halo approach (Seljak 2000, Ma & Fry 2000).

Figure 6 plots the resulting PVDF (in the LCDM model) at $r_{12} = 1h^{-1}$, $0.3h^{-1}$ and $0.1h^{-1}\text{Mpc}$ against the pairwise velocity v_{12} normalized by the PVD at each separation. We adopt the Press-Schechter mass function for definiteness. Note that the quantitatively similar behavior is obtained for other cosmological models, but with different PVDs. The PVDF for small separation pairs ($r_{12} \ll 1h^{-1}\text{Mpc}$) is well described by the exponential distribution. As r_{12} increases, the central region resembles the Gaussian distribution while the exponential tail is still clear at large velocities. Neither the inner nor outer slope of the density profile produces any systematic difference in the non-Gaussian tails of PVDF, in contrast to the single-particle velocity distribution in Figure 3. This qualitative behavior is in complete agreement with the result of Sheth (1996) assuming the scale-free model and the singular isothermal sphere. Therefore we conclude that the exponential distribution of the PVDF is a rather general consequence in the gravitational instability picture fairly independent of the underlying cosmological model.

3. Pairwise relative peculiar velocity dispersions

3.1. Dark matter particles

We have shown that the *shape* of the PVDF is well approximated by the exponential in a fairly insensitive manner to either the cosmological model or the dark halo density profile. Note, however, that this does not imply the PVD is determined independently of the cosmology, but

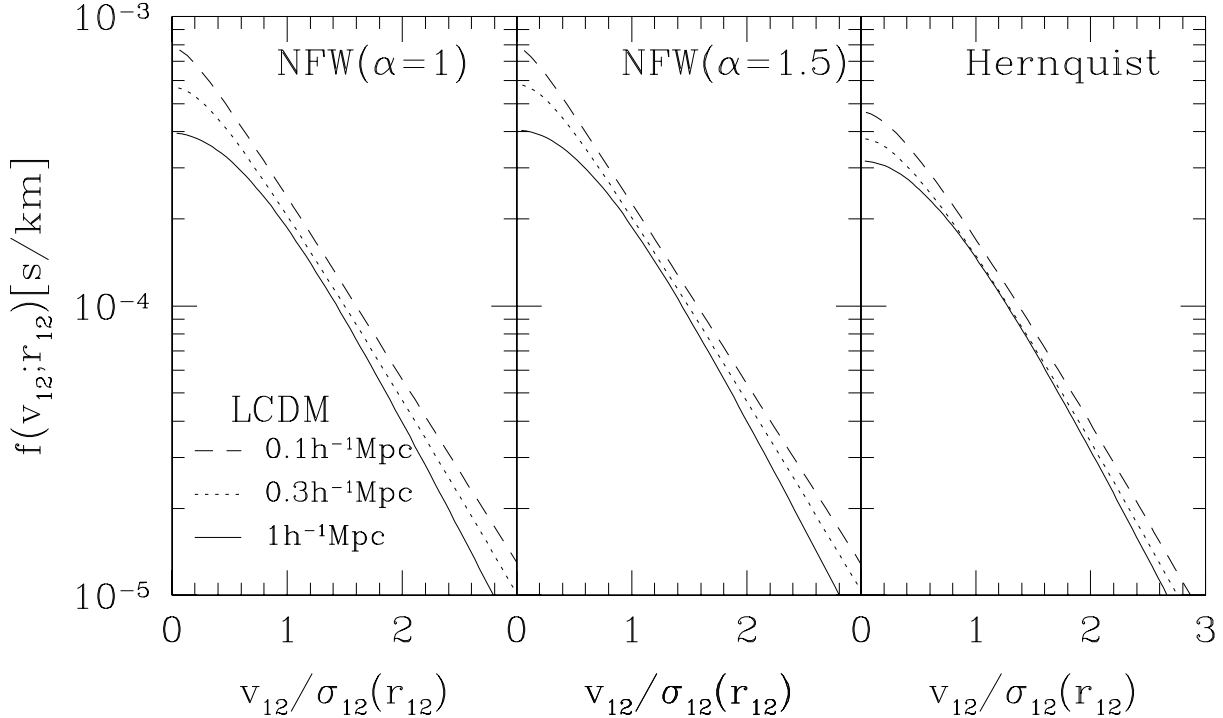


Fig. 6. Pairwise velocity distribution function averaged over the halo mass function in the LCDM universe. *Left:* NFW($\alpha=1$); *Middle:* NFW($\alpha=1.5$); *Right:* Hernquist profile. Solid, dotted and dashed lines indicate the results at the pair separation of $1h^{-1}\text{Mpc}$, $0.3h^{-1}\text{Mpc}$, and $0.1h^{-1}\text{Mpc}$.

rather it is the basic source for the cosmological model-dependence, through the mass function of halos. Since the PVDF is already obtained, one may evaluate the PVD $\sigma_{12}(r_{12})$ directly as

$$\sigma_{12}^2(r_{12}) = \int_{-\infty}^{\infty} dv_{12} f_{12}(v_{12}; r_{12}) v_{12}^2. \quad (17)$$

We note, however, that the above expression is valid only when the one-halo term $\xi_{1h}(r_{12})$ is sufficiently larger than unity. If one takes account of particle pairs residing in two different halos that we neglect in the present modeling, one should rather replace the normalization factor \tilde{N} by $1 + \xi(r_{12})$ since the factor physically corresponds to the relative probability of finding a pair at separation r_{12} . This consideration implies the normalization of the PVD from the one-halo contribution should be

$$\sigma_{12}^2(r_{12}) = \frac{\xi_{1h}(r_{12})}{1 + \xi(r_{12})} \int_{-\infty}^{\infty} dv_{12} f_{12}(v_{12}; r_{12}) v_{12}^2. \quad (18)$$

In fact, this agrees with equation (21) of Sheth et al. (2001). We compute the two-point correlation function, $\xi(r_{12}) = \xi_{1h}(r_{12}) + \xi_{2h}(r_{12})$, on the basis of the dark halo approach (Seljak 2000), and we also confirm that the resulting $\xi(r_{12})$ is in good agreement with the fitting formula of Peacock & Dodds (1996) by an appropriate choice of the concentration parameter $c(M)$ as discussed in subsection 2.1.

Figure 7 shows the PVD calculated according to equation (18). The comparison among

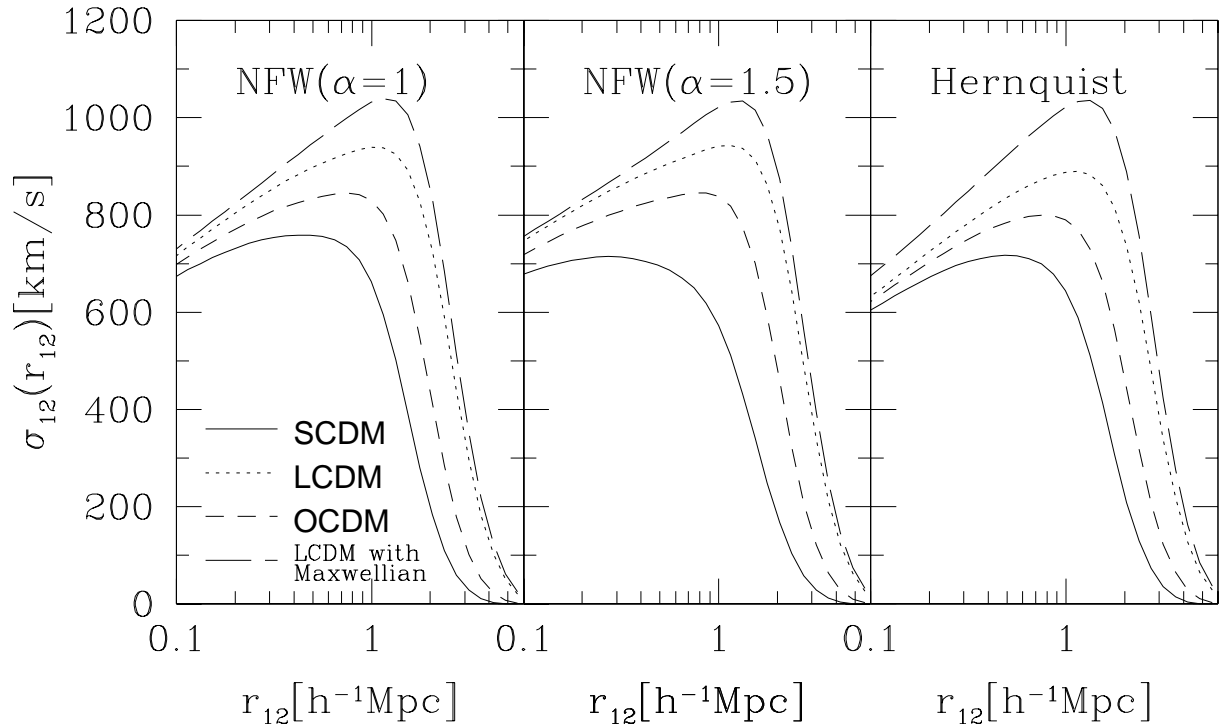


Fig. 7. The pairwise velocity dispersion of dark matter particles. *Left:* NFW($\alpha = 1$); *Middle:* NFW($\alpha = 1.5$); *Right:* Hernquist profile. Solid, dotted and dashed lines indicate the results in SCDM, LCDM, and OCDM. Long-dashed line shows the result in LCDM under the assumption that each halo has the Maxwellian velocity distribution function with constant velocity dispersion.

the different model predictions indicates that the amplitude of PVD sensitively depends on the cosmological parameters through the mass function $n(M)$, but is almost insensitive to the density profile of dark halo. Note, however, that this is partly because we have chosen the value of $c(M)$ so as to reproduce the same $\xi(r)$ irrespectively of the density profile. We also show the result with neglecting the scale-dependence of the velocity distribution in the case of the LCDM model (*long-dashed* lines). This indicates that the isothermal approximation (Sheth et al. 2001) is quite acceptable in predicting the PVD.

We attempted an empirical fitting to our numerical results at different redshifts (Fig.8) by adopting a power-law form:

$$\sigma_{12}(x_{12}) = A \left(\frac{x_{12}}{1h^{-1}\text{Mpc}} \right)^p, \quad (19)$$

in terms of the *comoving* pair separation $x_{12} \equiv r_{12}(1+z)$. The values of the amplitude A and the power-law index p fitted for $0.01h^{-1}\text{Mpc} < x_{12} < x_{\text{max}}$ are listed in Table 1 in the LCDM model, where x_{max} is the comoving separation at which the PVD becomes maximum. Since the two-halo term $\xi_{2h}(r_{12})$ becomes dominant contribution to $\xi(r_{12})$ for larger separations, equation (19) becomes inaccurate for $x > x_{\text{max}}$. The fit is accurate within 5%, which is comparable to the other systematic errors including the numerical integration or the Gaussian approximation. This

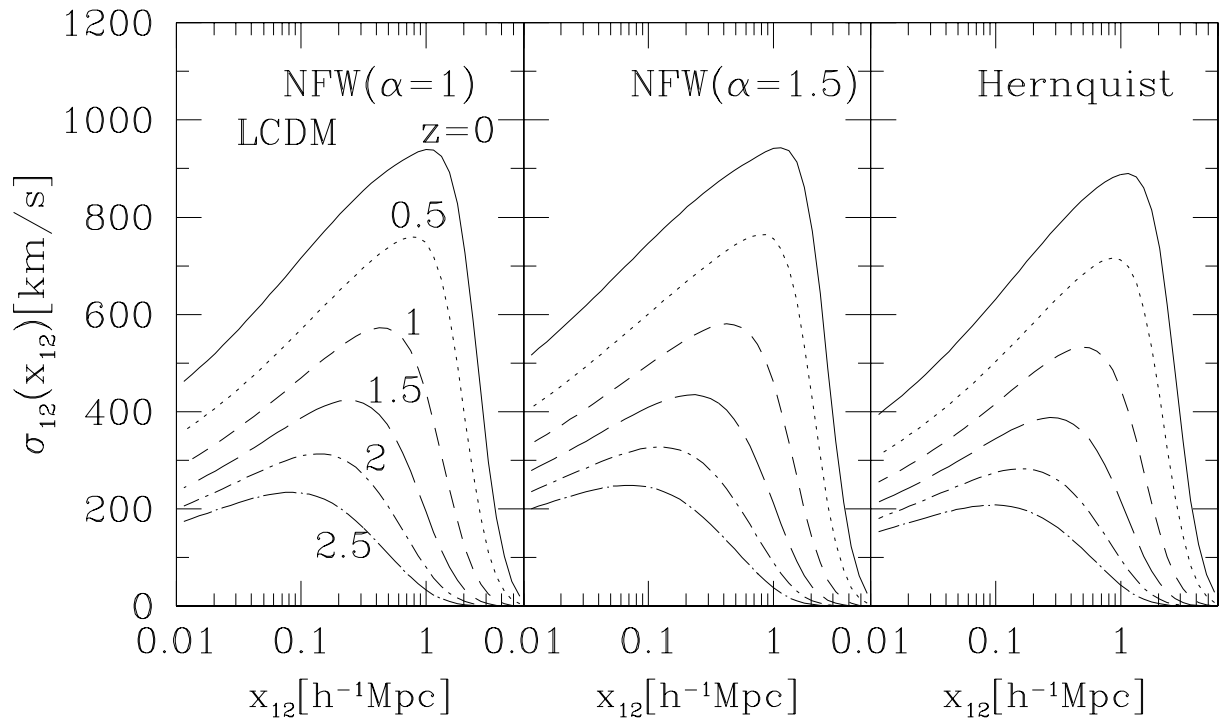


Fig. 8. The pairwise velocity dispersion of dark matter particles in LCDM at $z=0, 0.5, 1.0, 1.5, 2.0$ and 2.5 from top to bottom. *Left:* NFW($\alpha=1$); *Middle:* NFW($\alpha=1.5$); *Right:* Hernquist profile.

result may be compared with the independent prediction based on the cosmic virial theorem (Peebles 1976; Suto 1993; Suto & Jing 1997). For reference, if the correlation function of dark matter is given by $(r/5.4h^{-1}\text{Mpc})^{-1.8}$, the cosmic virial theorem implies that

$$v_{12}(r_{12})_{\text{CVT}} = 990 \left(\frac{\Omega_0}{0.3}\right)^{1/2} \left(\frac{Q}{2.0}\right)^{1/2} \left(\frac{r_{12}}{1h^{-1}\text{Mpc}}\right)^{0.1} \text{ km/s}, \quad (20)$$

where Q is the normalized amplitude of the three-point correlation function. The value of Q for dark matter clustering is somewhat uncertain, but may be close to 2 in LCDM (Suto 1993), and thus this estimate is fairly consistent with our prediction presented here.

Table 1. Power-law fits to the relative peculiar velocity dispersion in the LCDM model.

z	$x_{\text{max}}[h^{-1}\text{Mpc}]$	NFW($\alpha=1$)		NFW($\alpha=1.5$)		Hernquist	
		$A[\text{km/s}]$	p	$A[\text{km/s}]$	p	$A[\text{km/s}]$	p
0.0	1.0	1016	0.17	997	0.14	957	0.19
0.5	0.9	846	0.18	834	0.15	791	0.20
1.0	0.4	731	0.20	713	0.16	675	0.22
1.5	0.25	578	0.19	517	0.15	533	0.20
2.0	0.15	458	0.17	442	0.13	416	0.18
2.5	0.11	339	0.14	325	0.10	304	0.15

3.2. Effect of biasing

It is well known that the PVD of the observed galaxies is generally smaller than the value predicted in current popular models (e.g., Davis & Peebles 1983; Mo, Jing & Börner 1993; Suto 1993; Suto & Jing 1997). This may be interpreted as a manifestation of the spatial biasing of galaxies relative to dark matter.

Jing, Mo & Börner (1998) analyzed the Las Campanas Redshift Survey galaxies and developed a phenomenological biasing model, CLuster underWeight bias (CLW, hereafter) which successfully accounts for the amplitudes of the two-point correlation function and the PVD simultaneously. More recently Jing, Börner & Suto (2002) performed the similar analysis of galaxies in the PSCz catalog (Saunders et al. 2000) which are selected from the InfraRed Astronomical Satellite (IRAS) Point Source Catalog (PSC; Beichman et al. 1988). They found that the IRAS selected galaxies, which are likely to be dominated by late-types, have significantly smaller PVD than those in other catalogues. In addition, they applied the CLW bias scheme to mock samples from N -body simulations and concluded that the PVD of the PSCz galaxies is significantly smaller than those predicted from the CLW bias in the popular CDM models. In this subsection, we revisit this issue combining the biasing effect with our analytical model of the PVD in a complementary manner to the direct method using the N -body data.

The CLW scheme can be applied to our analytical model easily. According to Jing et al. (2002), we adopt that the selection function of galaxies in a halo of mass M is proportional to $(M/10^{14}M_{\odot})^{-\beta}$. This is simply equivalent to replacing the mass function $n(M)$ in equation (15) by $n(M)(M/10^{14}M_{\odot})^{-\beta}$. Because this biasing model puts lower weight on the massive clusters where the velocity dispersion is large, increasing β suppresses the mean PVD. In fact, the Las Campanas redshift survey data are consistent with $\beta = 0.08$, and the PSCz data prefer a much larger value $\beta = 0.25$. Physically speaking, this phenomenological prescription should be understood as the dependence of the efficiency of galaxy formation on the mass of the hosting halo.

In addition we consider another biasing to take into account the observed density-morphology relation of galaxies. Since spiral galaxies preferentially avoid the central region of massive clusters (i.e., halos in the present context), the PVD of spirals is generally suppressed especially in the case of the modified NFW profile that has stronger central concentration (c.f., Fig.4). We attempt to incorporate this effect by introducing the selection probability that depends on a distance from the center of the halo:

$$p(r|M) = a + \frac{r}{r_{\text{vir}}(M)}b. \quad (21)$$

We set $a = 0.2$ and $b = 0.6$ so as to reproduce the observed ratio of spirals to ellipticals; 2:8 in the inner part and 8:2 in the outer part. In practice, we calculate the PVD by replacing $\rho(r|M)$ by $\rho(r|M)p(r|M)$ in equation (18).

The results are shown in Figure 9 for the modified NFW profile in the LCDM model.

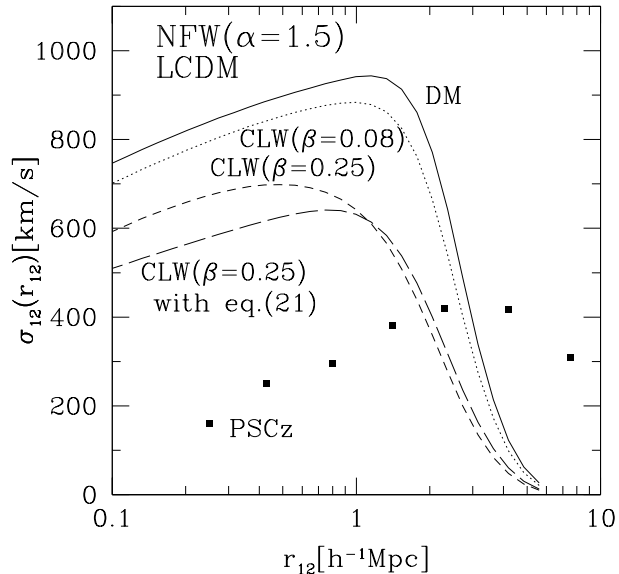


Fig. 9. Pairwise peculiar velocity dispersion for *galaxies* with empirical biasing scheme in LCDM; *Solid*: dark matter particles. *Dotted*: CLW with $\beta = 0.08$, *Short-dashed*: CLW with $\beta = 0.25$, *Long-dashed*: CLW with $\beta = 0.25$ and density-morphology relation. The filled squares indicate the values for the PSCz galaxies estimated by Jing et al. (2002).

The dotted and short-dashed lines represent the results taking account of the CLW bias effect while the long-dashed lines consider the density-morphology relation (eq.[21]) in addition to the CLW bias. The degree of suppression of the PVD is in agreement with the simulation results of Jing et al. (2002). Even with the density-morphology relation, the PVD of the IRAS PSCz galaxies is too small to be reconciled in the current model as Jing et al. (2002) claimed.

4. Summary

We have presented a detailed prediction for the pairwise peculiar velocity distribution function (PVDF) applying the dark matter halo approach. In particular, we have derived the PVDF in a direct and self-consistent manner with the assumed density profile for dark matter halo for the first time. On the other hand, we neglect the halo-halo contribution assuming that any pair of particles resides in a common halo. Thus our predictions are quantitatively valid only on small scales $\lesssim 1h^{-1}\text{Mpc}$, but our result turns out to be fairly close to the previous one by Sheth (1996) and Sheth et al. (2001) who assumed the *isothermal* velocity distribution in a single halo. In this sense, our independent approach may be regarded as to provide an empirical justification for their simplifying assumptions, and also our predictions are fairly accurate on those small scales.

We have shown that the shape of the PVDF is well approximated by the exponential in a fairly insensitive manner to either the cosmological model or the dark halo density profile. The dependence on the PVD on the halo density profiles that we employed is also fairly small,

yielding the difference less than about 10 percent.

We have also obtained a practical fitting formula for the PVD of dark matter particles (eq.[19]) at different cosmological models as a function of the pair separation. This may be useful in modeling redshift-space distortion of clustering. The result is in reasonable agreement with the estimate on the basis of the cosmic virial theorem. Furthermore we apply an empirical biasing scheme into our model and attempt to predict the PVD of *galaxies*. We can reproduce the previous simulation results on the basis of our analytical method, and also confirmed that the very small PVD estimated for the PSCz galaxies (Jing et al. 2002) is difficult to be reconciled with a simplistic biasing model and/or the underlying CDM model.

The discrepancy between the prediction and the observation shown in section 3.2 indicates the presence of velocity bias, in addition to the other selection effects. In fact, each luminous galaxy is a clump composed of the baryon as well as dark matter particles, whose bulk motion might not trace the random motion of the individual dark matter particles. In this case, the galaxy-galaxy interaction through tidal field or gas pressure of baryon might be an important source for velocity bias. At least, our present treatment using dark matter halo approach can provide a quantitative prediction for the PVD of the dark matter particles. Therefore next step, the effect of velocity bias including these interactions should be incorporated into our scheme to account for the PVD of the galaxies.

T. K. thanks Chiaki Hikage, Issha Kayo, and Masamune Oguri for discussions and comments on the manuscript. This research was supported in part by Monbu-Kagakusho (07CE2002, 12640231).

References

- Beichman, C. A., Neugebauer, G., Habing, H. J., Clegg, P. E., & Chester, T. J. 1988, IRAS Catalogs and Atlases, Vol.1: Explanatory Supplement (JPL)
- Binney, J., & Tremaine, S. 1987, Galactic Dynamics (Princeton university press, Princeton)
- Bullock, J. S., Kolatt, T. S., Sigad, Y., Somerville, R. S., Kravtsov, A. V., Klypin, A., Primack, J. P., & Dekel, A. 2001, MNRAS, 321, 559
- Davis, M., & Peebles, P. J. E. 1983, ApJ, 267, 465
- Diaferio, A., & Geller, M. J. 1996, ApJ, 467, 19
- Efstathiou, G. P., Frenk, C. S., White, S. D. M., & Davis, M. 1988, MNRAS, 235, 715
- Fisher, K. B., Davis, M., Strauss, M. A., Yahil, A., & Huchra, J. P. 1994, MNRAS, 267, 927
- Fukushige, T., & Makino, J. 1997, ApJ, 477, L9
- Fukushige, T., & Makino, J. 2001a, ApJ, 557, 533
- Fukushige, T., & Makino, J. 2001b, ApJL, submitted (astro-ph/0108014)
- Hanyu, C., Habe, A., 2001, ApJ, 554, 1268
- Hernquist, L. 1990, ApJ, 356, 359

Jing, Y. P., Börner, G., & Suto, Y. 2002, ApJ, 564, 15
Jing, Y. P., Mo, H. J., & Börner, G. 1998, ApJ, 494, 1
Jing, Y. P., & Suto, Y. 2000, ApJ, 529, L69
Juszkiewicz, R., Fisher, K. B., & Szapudi, I. 1998, ApJ, 504, L1
Kitayama, T., & Suto, Y. 1996, ApJ, 469, 480
Kitayama, T., & Suto, Y. 1997, ApJ, 490, 557
Ma, C. P., & Fry, J. N. 2000, ApJ, 543, 503
Marzke, R. O., Geller, M. J., Da Costa Costa, M. L., Huchra, J. P. 1995, AJ, 110, 477
Mo, H.J., Jing, Y. P., Börner, G. 1993, MNRAS, 264, 825
Mo, H.J., Jing, Y. P., Börner, G. 1997, MNRAS, 286, 979
Moore, B., Governato, F., Quinn, T., Stadel, J., & Lake, G. 1998, ApJ, 499, L5 MNRAS, 310, 1147
Natarajan, P., Hjorth, J., & van Kampen, E. 1997, MNRAS, 286, 329
Navarro, J. F., Frank, C. S., & White, S. D. M. 1996, ApJ, 462, 563
Navarro, J. F., Frank, C. S., & White, S. D. M. 1997, ApJ, 490, 493
Oguri, M., Taruya, A, Suto, Y. 2001, ApJ, 559, 572
Peacock, J. A., & Dodds, S. J. 1996, MNRAS, 280, L19
Peebles, P.J.E. 1976, Astrophys.Sp.Sci., 45, 3
Press, W., & Schechter, P. 1974, ApJ, 187, 425
Saunders, W., Sutherland, W. J., Maddox, S. J., Keeble, O., Oliver, S. J., Rowan-Robinson, M.,
McMahon, R. G., Efstathiou, G. P. et al. 2000, MNRAS, 317, 55
Seljak, U. 2000, MNRAS, 318, 203
Seto, M., & Yokoyama, J. 1998, ApJ, 492, 421
Sheth, R. K. 1996, MNRAS, 279, 1310
Sheth, R.K., & Diaferio, A. 2001, MNRAS, 322, 901
Sheth, R. K., Hui, L., Diaferio, A., & Scoccimarro, R. 2001, MNRAS, 325, 1288
Suto Y. 1993, Prog.Theo.Phys., 90, 1173
Suto Y. & Jing, Y.P. 1997, ApJS, 110, 167 ApJ, 431, 559